

Variational Quantum Eigensolver for $SU(N)$ Fermions

Mirko Consiglio,^{1,*} Wayne J. Chetcuti,^{2,3,4} Carlos Bravo-Prieto,^{4,5} Sergi Ramos-Calderer,^{4,5} Anna Minguzzi,⁶ José I. Latorre,^{4,5,7} Luigi Amico,^{4,7,8,9} and Tony J. G. Apollaro^{1,†}

¹*Department of Physics, University of Malta, Msida MSD 2080, Malta*

²*Dipartimento di Fisica e Astronomia, Via S. Sofia 64, 95127 Catania, Italy*

³*INFN-Sezione di Catania, Via S. Sofia 64, 95127 Catania, Italy*

⁴*Quantum Research Centre, Technology Innovation Institute, Abu Dhabi, UAE*

⁵*Departament de Física Quàntica i Astrofísica and Institut de Ciències del Cosmos (ICCUB),*

Universitat de Barcelona, Martí i Franquès 1, 08028 Barcelona, Spain.

⁶*Université Grenoble Alpes, CNRS, LPMMC, 38000 Grenoble, France*

⁷*Centre for Quantum Technologies, National University of Singapore, 3 Science Drive 2, Singapore 117543, Singapore*

⁸*CNR-MATIS-IMM & INFN-Sezione di Catania, Via S. Sofia 64, 95127 Catania, Italy*

⁹*LANEF 'Chaire d'excellence', Université Grenoble Alpes, CNRS, 38000 Grenoble, France*

(Dated: November 24, 2021)

Variational quantum algorithms aim at harnessing the power of noisy intermediate-scale quantum computers, by using a classical optimizer to train a parameterized quantum circuit to solve tractable quantum problems. The variational quantum eigensolver is one of the aforementioned algorithms designed to determine the ground-state of many-body Hamiltonians. Here, we apply the variational quantum eigensolver to study the ground-state properties of N -component fermions. With such knowledge, we study the persistent current of interacting $SU(N)$ fermions, which is employed to reliably map out the different quantum phases of the system. Our approach lays out the basis for a current-based quantum simulator of many-body systems that can be implemented on noisy intermediate-scale quantum computers.

I. INTRODUCTION

The current information technology era is being reshaped by emerging quantum technologies in fields ranging from cryptography to computation. In this context, noisy intermediate-scale quantum (NISQ) computers may already provide useful applications before fault-tolerant quantum computation is realized [1, 2].

Interacting many-body ground-states and quantum phases of matter define important domains in which NISQ devices could play a pivotal role. The necessary steps in order to address a many-body problem via a quantum computer consist of representing the system under scrutiny in terms of qubits, and executing an efficient algorithm to compute the quantity of interest. The system's specific qubit representation has to be devised carefully to optimize the complexity of the resulting quantum circuit. Similarly, a great variety of algorithms have been proposed, and variational quantum algorithms are characteristic examples in the NISQ era exploiting the quantum advantage provided by few-body, noisy quantum computers working alongside classical computers [3].

The Hubbard model, originally introduced to study the dynamics of electrons in solids [4], is a paradigmatic example in addressing the physical properties of strongly interacting quantum many-body systems, ranging from superconductivity to quantum magnetism [5]. The Hubbard model describes itinerant electrons sensing a local interaction. With cold atom quantum technology, the

Hubbard model can be studied with unprecedented control, and flexibility of the system's physical conditions [6–9]. Despite the simple logic implied in the Hubbard Hamiltonian dynamics, finding its ground-state poses a challenging problem in many-body physics, whose solution has been attempted numerous times by exploiting the most advanced available methods [10]. With no exception, different quantum algorithms have been devised to address the problem [11–18], mainly focusing on determining the ground-state via the application of the aforementioned variational quantum algorithms.

Here, we apply the variational quantum eigensolver (VQE) [19] to $SU(N)$ Hubbard type models, describing strongly interacting fermions with N spin-components. Interacting $SU(N)$ fermions play an important role in a variety of different contexts ranging from high energy [20, 21] to specific situations in condensed matter physics [22–25]. The higher symmetry accounts for a variety of novel phenomena, such as symmetry protected topological phases, and Mott-insulator transitions at finite interaction values [26]. Recently, the research scope on $SU(N)$ fermions has been substantially enlarged by cold atom quantum technology [27, 28]. Specifically, experiments with alkaline-earth and ytterbium atoms have simulated $SU(N)$ fermions [29–31] with N as large as ten. $SU(N)$ cold atoms at the mesoscopic scale can provide a new platform for atomtronic circuits to widen the scope of current quantum simulation and access quantum devices with new specifications [32]. In particular, by using the logic of current-voltage characteristics of solid state physics, an important goal of the atomtronics field is to eventually exploit matter-wave currents to probe quantum phases of matter. For $SU(N)$ fermions, such

* mirko.consiglio.16@um.edu.mt

† tony.apollaro@um.edu.mt

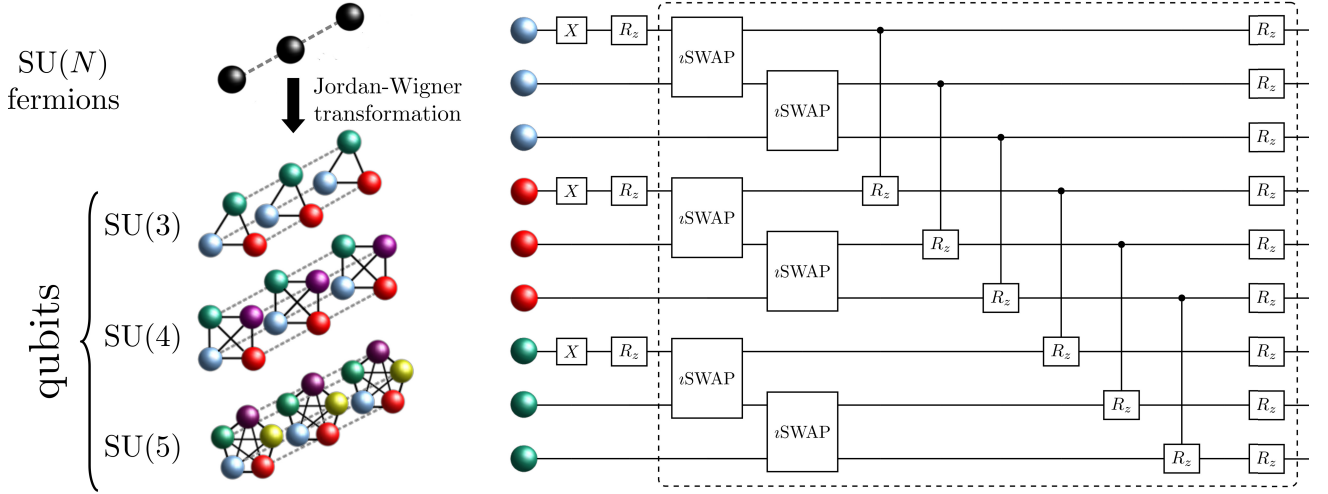


FIG. 1. Parameterized quantum circuit employed for the VQE. (Left) Mapping an 3-site linear $SU(N)$ Hubbard Hamiltonian (black spheres) with only nearest-neighbor hopping and on-site interaction to an N -sided qubit prism of length L . The dashed gray lines represent the hopping term t between same-color qubits, and continuous black lines the on-site interaction U . (Right) Parameterized quantum circuit for the 3-site $SU(3)$ Hubbard Hamiltonian in the $N_p = 3$ (number of particles) sector starting from a state with all fermions on the same site. The variational parameters of the parameterized quantum circuit are contained within the $iSWAP$, controlled- R_z and R_z gates. The dashed box corresponds to one variational circuit layer. Note that the last sequence of entangling gates can be mostly applied in parallel.

a program has been initiated by studying the persistent current [33].

In this paper, we access the persistent current by means of a VQE. To this end, we generalize the Jordan-Wigner transformation applied to two spin-component fermions [34, 35] to $SU(N)$ fermions. We apply our fermion-to-qubit mapping to $SU(N)$ Hubbard models in which a density-density repulsion is also considered, further to the characteristic local interaction. By careful analysis of the complexity and performance of the VQE, we demonstrate that the quantum correlations characterizing the ground-state of system can be captured only if quantum circuits with a suitable depth are considered. We shall see that $SU(N)$ fermionic systems require a larger number of layers with respect to two-component fermionic systems, and how the persistent current displays distinctive features in the different quantum phases of the system.

II. $SU(N)$ FERMION-TO-QUBIT MAPPING

Our physical system is made of a set of $SU(N)$ fermions localized in a 1D ring lattice with L sites:

$$H = -t \sum_{i=1}^L \sum_{s=1}^N \left(e^{i \frac{2\pi\phi}{L}} c_{i,s}^\dagger c_{i+1,s} + \text{h.c.} \right) + U \sum_{i=1}^L \sum_{s=1}^N \sum_{s'=s+1}^N n_{i,s} n_{i,s'} + V \sum_{i=1}^L n_i n_{i+1}, \quad (1)$$

where $c_{i,s}^\dagger$ ($c_{i,s}$) creates (annihilates) a fermion with spin-component s at site i . The s -fermion number operator is $n_{i,s} = c_{i,s}^\dagger c_{i,s}$, with the total number operator defined as $n_i = \sum_s n_{i,s}$ on site i . The parameter t is the hopping amplitude of a fermion between nearest-neighbor sites, while the parameters U and V describe the on-site and density-density nearest-neighbor interaction, respectively. In this paper, only systems with singlet states for which the total magnetization $S^z = 0$ (equal population in each color) are considered. Furthermore, we only consider non-negative values for both U and V .

For $V = 0$, a superfluid to Mott insulator transition takes place for a finite value of the local repulsive interaction U [26, 36]. Such a transition occurs at finite U for $N > 2$. Because of the interplay between U and V , different quantum phases can be displayed. Specifically, the phase diagram involves a superfluid phase, a Mott phase, and a ‘beat’ phase in which the particle occupation is modulated along the chain with a vanishing spin gap [37].

The phase factor $e^{i \frac{2\pi\phi}{L}}$ in Eq. (1) takes into account the effective magnetic flux piercing the ring, which is able to impart a persistent current with the following form:

$$I(\phi) = \frac{2\pi t}{L} \sum_{i=1}^L \sum_{s=1}^N \langle \psi_0 | e^{i \frac{2\pi\phi}{L}} c_{i,s}^\dagger c_{i+1,s} - \text{h.c.} | \psi_0 \rangle, \quad (2)$$

where $|\psi_0\rangle$ denotes the ground-state of Eq. (1). For the case of $V = 0$, it has been recently demonstrated that as a combination of the interaction, magnetic flux and

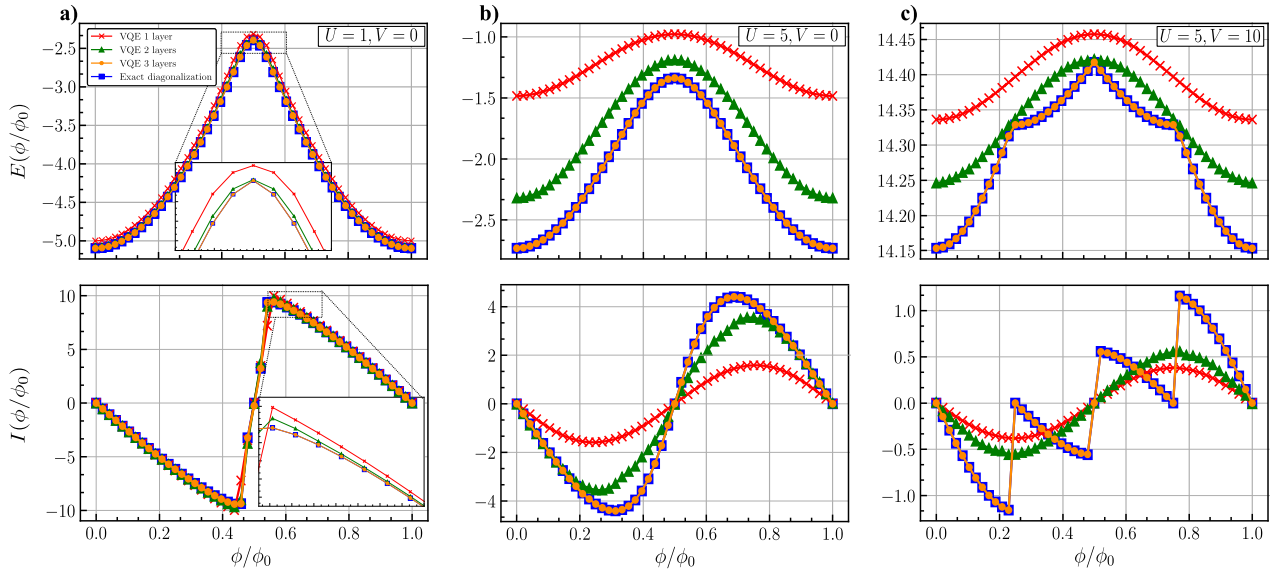


FIG. 2. The ground-state energy $E_0(\phi)$ (top panel) and the corresponding persistent current $I(\phi)$ (bottom panel) for SU(3) fermions with different local U and nearest-neighbor V interactions, in the dilute filling regime of the Hubbard model. The profile of the persistent current gives a clear indication between the **a**) superfluid, **b**) Mott and **c**) beat phases. Exact diagonalization for $L = N_p = 3$ is used to monitor the results obtained by the VQE. Three layers are required in order for the ground-state energy of the latter to match the former.

spin correlations, the effective elementary flux quantum ϕ_0 which fixes the persistent current periodicity, is observed to evolve from a single particle one to an extreme case of fractional flux quantum, in which one flux quantum is shared by all the particles. Such a phenomenon reflects a type of attraction from repulsion: despite the repulsive interaction, spin correlations can lead to many-body states reacting as if they were bound states of fermions [33].

To implement the VQE on a NISQ computer, it is crucial to represent the system described by Eq. (1) in terms of qubits [12, 13, 38, 39]. To this end, we extend the Jordan-Wigner transformation originally devised for two-component fermions [34, 35, 40] to the general SU(N) case. We introduce N sets of Pauli operators, one for every spin-component s , hereafter called color, of the fermionic atom. The mapping assumes the following form:

$$c_{i,s}^\dagger = \prod_{j < n} \sigma_j^z \sigma_n^+, \quad (i, s) \rightarrow n = i + sL. \quad (3)$$

In this way, up to the standard Pauli-string operator $\prod_{j < n} \sigma_j^z$, a fermion of color s on site i is mapped onto a spin- $\frac{1}{2}$ operator σ_n^+ acting on site $n = i + sL$ (of the qubit lattice). As a consequence, a system of N_p SU(N) fermions on L sites is mapped into NL qubits, where N_p is the number of particles. It is straightforward to show that the mapping in Eq. (3) preserves fermionic commutation rules independently of the chosen order of the color s appearing in the definition of n . In the following, without loss of generality, we adopt an increasing order for s , meaning $n' > n$ for fermionic operators with $s' > s$. The

Hamiltonian of Eq. (1) is thus mapped to

$$H = -t \sum_{i,s} (\sigma_{i+sL}^+ \sigma_{i+sL}^- + \text{h.c.}) \prod_{j=i+1+sL}^{i-1+sL} \sigma_j^z + \frac{U}{4} \sum_{i,s < s'} (1 - \sigma_{i+sL}^z) (1 - \sigma_{i+s'L}^z) + \frac{V}{4} \sum_{i,s,s'} (1 - \sigma_{i+sL}^z) (1 - \sigma_{i+s'L}^z). \quad (4)$$

The aim of the VQE is to find a set of parameters $\vec{\theta}$ able to obtain a quantum state $|\psi(\vec{\theta})\rangle$, that minimizes the expectation value of the energy $E(\vec{\theta})$ of a Hamiltonian, through a shallow parameterized quantum circuit $U(\vec{\theta})$ acting on an initial state $|\psi\rangle$. The optimization is achieved through an adiabatically-assisted quantum-classical loop of a classical minimization process using evaluations of the parameterized quantum circuit [41]. We propose a variational ansatz inspired by the extension of the Jordan-Wigner transformation to SU(N) fermions, that can be seen in Fig. 1, by adopting a number-preserving ansatz using parameterized i SWAP gates as a model for the hopping terms between sites representing the same color. The interaction terms, as well as the on-site terms, between fermions of a different color, are represented by controlled- R_z and R_z gates, respectively.

We have simulated the quantum circuits using the Qibo API [42, 43], disregarding the influence of noise and the impact of finite sampling. The classical optimization technique employed in the quantum-classical loop is the BFGS method [44], a gradient-based approach, which in-

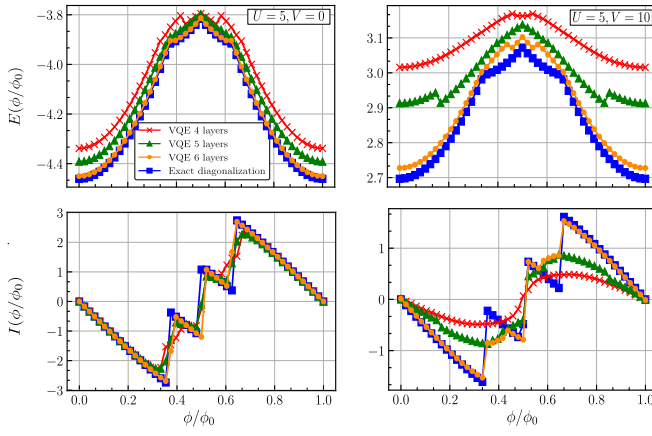


FIG. 3. The ground-state energy $E_0(\phi)$ (top panel) and the corresponding persistent current $I(\phi)$ (bottom panel) for $SU(3)$ fermions with different local U and nearest-neighbor V interactions, in the dilute filling regime of the Hubbard model. Exact diagonalization for $L = 5$ and $N_p = 3$ is used to monitor the results obtained by VQE.

volves the computation of the inverse Hessian matrix. Finally, we benchmark our results using the exact diagonalization methods provided by the QuSpin software package [45, 46]. In our approach, we monitor the persistent current given in Eq. (2), that we access by means of a VQE subroutine.

III. RESULTS

First, we discuss the results of the VQE for commensurate and incommensurate $SU(3)$ models found in Figs. 2 and 3, respectively, with different values of the parameters U and V corresponding to different physical regimes in the phase diagram of the system. At $\phi = 0$, the final optimal parameters of each case were determined by training the VQE with random initialization. However, each subsequent instance of the VQE, tasked with finding the ground-state energy of the model with the next iteration of ϕ , was fed the optimal parameters from the previous instance. This form of adiabatic assistance, along with the symmetry of the ground-state energy along the degeneracy point $\phi/\phi_0 = 0.5$, offers a significant speed up in mapping out the ground-states of the extended Hubbard Hamiltonian over the entire range of ϕ , which is necessary for determining the persistent current.

In the lower panels of Figs. 2 and 3 we monitor the persistent current given in Eq. (2). We notice that the discontinuities of $I(\phi)$, resulting from energy level crossings by varying ϕ , are fully captured, indicating the occurrence of spinon creation in the ground-state [33]. We note that such a phenomenon is only captured by the VQE if a sufficient number of layers are considered. This feature is consistent with the general theory signifying that the flux quantum fractionalization is a genuine many-body correlation effect. We also notice that, for small U and

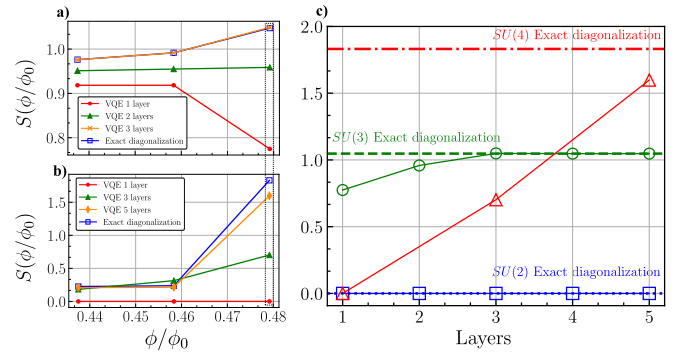


FIG. 4. Values for the bipartite entropy $S(\phi)$ of half the qubit chain for **a**) $SU(3)$ and **b**) $SU(4)$ for an increasing number of ansatz layers for a Hubbard model with $U = 1$ and $V = 0.5$ at commensurate fillings, namely, $N_p = N$. **c**) A detail on $\phi = 0.5$ can be seen where $SU(2)$ and $SU(3)$ examples quickly reach the entropy of the exact diagonalization state, while the $SU(4)$ case still requires more correlations to be built up within the quantum circuit to fully approximate the ground-state (see Fig. 8 in the Appendix).

V , a shallow circuit estimates the ground-state with high accuracy. However, the correlations that are present for larger U and V necessitate more ansatz layers to fully capture the ground-state of the model. We use the entanglement entropy of the final state as an additional measure to gauge how closely the VQE reproduces the desired ground-state.

We note that by increasing the number of layers of the parameterized quantum circuit, the entanglement in the ground-state increases, as shown in Fig. 4. This layer-by-layer build up of entanglement is crucial to capture the correlations of the target quantum state. It is only after the parameterized quantum circuit has enough depth to reach the target entanglement entropy, that the VQE can start to approximate the target observable with high precision, as previously shown in Ref. [47]. We observe that correctly taking the ground-state entanglement into account is very important to capture the physics of the system.

The number-preserving ansatz we introduce explores a subspace of the Hilbert space of size $\prod_{s=1}^N \binom{L}{N_s}$ for $SU(N)$ fermions in L sites, where N_s is the number of fermions of color s . Therefore, the number of layers needed to properly capture the ground-state energy will depend on the expressibility of this ansatz in covering the reduced subspace. In order to reduce the number of parameters needed for the VQE, one could introduce a translationally invariant ansatz, to account for the periodic nature of the fermionic chains studied. If, as in our examined models (Figs. 2 and 3), we suppose that $N_s = N_{s'}$ for all colors s and s' , then this symmetry reduces the relevant basis of the problem to L^{N-1} states. However, this ansatz would need non-trivial and non-local quantum gates, which are not suitable for implementation in NISQ computers.

IV. CONCLUSION

In this work, we simulated a VQE program on $SU(N)$ fermions. As an important technical step, we extended the Jordan-Wigner transformation to N -component fermions. Our work provides a specific instance of a current-based quantum simulator: the physics of the system is probed by the current response to the gauge field. Specifically, we consider a 1D ring lattice of the Hubbard type, and we monitor the persistent current.

We have then applied the $SU(N)$ fermion-to-qubit mapping, using it to determine the ground-state energy of the Hubbard Hamiltonian via the VQE. We have found that the ground-state energy can be approached by utilizing a number-preserving ansatz, similarly to what is done for the $SU(2)$ case [12]. However our ansatz is generalized to the $SU(N)$ fermion case, and optimized to minimize the depth, and the number of gates and parameters needed to achieve the ground-state of the magnetic-flux-induced extended Hubbard Hamiltonian. In this context, it would be interesting to consider $SU(N)$ generalization of other two-component fermion-to-qubit mappings, such as the Bravyi-Kitaev [48] and Ball-Verstraete-Cirac [49, 50] encodings. Further optimization to this model would include the so-called state preparation and measurement mitigation [51], contextual optimization [52], implementation of exchange symmetries [53, 54], noise tailoring through randomization protocols [55], and noise-aware logical-to-physical qubit mappings [56] when running on quantum hardware. These methods for minimizing noise could be investigated and applied to the proposed parameterized quantum circuit, in order to obtain a further optimized algorithm for the determination of the ground-state energy of the Hubbard Hamiltonian (and other similar quantum models) on NISQ computers.

In view of the recent interest for the $SU(N)$ Hubbard model, motivated both by its experimental realization with cold atoms, and its relevance in modeling mesoscopic quantum devices stemming from the rapidly developing atomtronics technology, our work opens this model for investigation via variational quantum algorithms. At the same time, the proposed $SU(N)$ fermion-to-qubit mapping may prove useful in addressing the Hubbard model via classical algorithms originally developed for $SU(2)$ models, such as tensor network states [57], and specifically, Ppdf [58], providing further incentive in investigating some of the results obtained in this paper

The code is publicly available on [GitHub](#) [59].

ACKNOWLEDGEMENTS

We acknowledge fruitful discussions with Tobias Haug.

APPENDIX

A. Details on the $SU(N)$ Fermion-to-Qubit Mapping

The Hubbard Hamiltonian in Eq. (1) can be generalized to incorporate symmetric long-range hopping and interaction terms, transforming into

$$H = - \sum_{i=1}^L \sum_{r=1}^{\lfloor \frac{L}{2} \rfloor} \sum_{s=1}^N t_r \left(e^{i \frac{2\pi\phi}{L}} c_{i,s}^\dagger c_{i+r,s} + \text{h.c.} \right) + U \sum_{i=1}^L \sum_{r=1}^{\lfloor \frac{L}{2} \rfloor} \sum_{s=1}^N \sum_{s'=s+1}^N n_{i,s} n_{i,s'} + \sum_{i=1}^L \sum_{r=1}^{\lfloor \frac{L}{2} \rfloor} V_r n_i n_{i+r}, \quad (5)$$

where t_r is the hopping amplitude of a fermion between sites at a distance r , U is the on-site interaction, and V_r is the interaction between fermions at a distance r , with r being at most $\frac{L}{2}$ due to the closed nature of the model.

Given that the $SU(N)$ fermion-to-qubit mapping is independent of the parameters of the Hamiltonian, Eq. (5) (containing both site-dependent long-range hopping and interaction terms) can also be mapped to a qubit Hamiltonian, although with different geometry and interaction patterns:

$$H = - \sum_{i,s,r} t_r \left(e^{i \frac{2\pi\phi}{L}} \sigma_{i+sL}^+ \sigma_{i+r+sL}^- + \text{h.c.} \right) \prod_{j=i+1+sL}^{i+r-1+sL} \sigma_j^z + \frac{U}{4} \sum_{i,s < s'} (1 - \sigma_{i+sL}^z) (1 - \sigma_{i+s'L}^z) + \sum_{i,r,s,s'} \frac{V_r}{4} (1 - \sigma_{i+sL}^z) (1 - \sigma_{i+r+s'L}^z), \quad (6)$$

B. VQE Implementation

Determining the ground-state energy of the Hubbard model requires the generation of an initial state, and a parameterized quantum circuit able to modify the quantum state, with observable measurements efficiently calculating the expectation value of the ground-state. As the number of fermions for each color is conserved, the spin configuration of the initial state, i.e. the number of qubits in the $|1\rangle$ state, must be preserved with regards to the mapping. As a consequence, the quantum gates (unitary operations) in the parameterized quantum circuit must be in the form of Pauli terms present in the Hubbard Hamiltonian. Note that the ladder operators of the transformed hopping terms can be rewritten in terms of X and Y Pauli operators (ignoring qubit indices and Z operators without loss of generality) as follows:

$$\begin{aligned}
(e^{i\frac{2\pi\phi}{L}}\sigma^+\sigma^- + e^{-i\frac{2\pi\phi}{L}}\sigma^-\sigma^+) &= e^{i\frac{2\pi\phi}{L}}\frac{(X+iY)}{2}\frac{(X-iY)}{2} + e^{-i\frac{2\pi\phi}{L}}\frac{(X-iY)}{2}\frac{(X+iY)}{2} \\
&= \frac{1}{4}\left(e^{i\frac{2\pi\phi}{L}}(XX - iXY + iYX + YY) + e^{-i\frac{2\pi\phi}{L}}(XX + iXY - iYX + YY)\right) \\
&= \frac{1}{4}\left(\left(e^{i\frac{2\pi\phi}{L}} + e^{-i\frac{2\pi\phi}{L}}\right)(XX + YY) - i\left(e^{i\frac{2\pi\phi}{L}} - e^{-i\frac{2\pi\phi}{L}}\right)(XY - YX)\right) \\
&= \frac{1}{2}\left(\cos\left(\frac{2\pi\phi}{L}\right)(XX + YY) + \sin\left(\frac{2\pi\phi}{L}\right)(XY - YX)\right). \tag{7}
\end{aligned}$$

$$\begin{pmatrix} 1 & 0 & 0 & 0 \\ 0 & \cos(\theta) & -i\sin(\theta) & 0 \\ 0 & -i\sin(\theta) & \cos(\theta) & 0 \\ 0 & 0 & 0 & 1 \end{pmatrix} = \begin{array}{c} \text{---} \\ \text{---} \\ \text{---} \\ \text{---} \end{array} \boxed{\iota\text{SWAP}(\theta)} \begin{array}{c} \text{---} \\ \text{---} \\ \text{---} \\ \text{---} \end{array}$$

FIG. 5. Hopping term represented by the ιSWAP gate.

$$\begin{pmatrix} 1 & 0 & 0 & 0 \\ 0 & 1 & 0 & 0 \\ 0 & 0 & e^{-i\theta} & 0 \\ 0 & 0 & 0 & e^{i\theta} \end{pmatrix} = \begin{array}{c} \text{---} \\ \text{---} \\ \text{---} \\ \text{---} \end{array} \boxed{R_z(\theta)} \begin{array}{c} \text{---} \\ \text{---} \\ \text{---} \\ \text{---} \end{array}$$

FIG. 6. Interaction term represented by the controlled- R_z gate.

$$\begin{pmatrix} e^{-i\theta} & 0 \\ 0 & e^{i\theta} \end{pmatrix} = \boxed{R_z(\theta)} \begin{array}{c} \text{---} \\ \text{---} \end{array}$$

FIG. 7. On-site term represented by the R_z gate.

With these operators, we can finally assemble the parameterized quantum circuit for the determination of the ground-state of the Hubbard model, as shown in Fig. 1. In Figs. 5, 6, and 7, we present the quantum gates describing the hopping, interaction and on-site terms, respectively.

1. Circuit Complexity

Here we will give a brief analysis of basis gate decompositions where we assume that the native gate set is composed of any one-qubit gate and controlled-NOT (CNOT) gates. For the sake of simplicity, in the following we determine the effective circuit depth of a single ansatz layer, by assuming that the gate times and errors of one-qubit gates are significantly less than those of a typical CNOT gate [60]. A single ansatz layer consists of a one-qubit sublayer composed of R_z gates, with the first entangling sublayer incorporating the hopping terms, followed by the sublayer containing the interaction terms.

Each ιSWAP gate introduces three CNOT gates [61],

while each interaction term consisting of a controlled- R_z gate decomposes into two CNOT gates [62]. Thus, the hopping sublayer consists of $N(L-1)$ ιSWAP gates and the interaction sublayer is composed of $L(N-1)$ controlled- R_z gates. Therefore, the total number of decomposed CNOT gates is equal to $5NL - 3N - 2L$. Looking at the circuit depth, The hopping sublayer garners a depth of $3(L-1)$, with the interaction sublayer achieving a depth of $2(N-1)$. Hence, the effective depth of the parameterized quantum circuit is equal to $2N + 3L - 5$. Now counting the number of parameters, The hopping sublayer consists of $N(L-1)$ parameters, with each one-qubit sublayer having NL parameters, while the interaction sublayer consists of $L(N-1)$ parameters. Thus, each ansatz layer incorporates $3NL - N - L$ parameters, along with the last one-qubit sublayer introducing an extra NL parameters at the end of the circuit.

In each instance of the VQE, we considered an initial state starting in the computational basis equating to the spin configuration of the intended model. In fact, this ansatz allows for the simple notion of error detection to be implemented: by checking the Hamming weight (the number of 1s in the binary result) of the output and confirming that it is conserved with respect to each individual spin color. If a non-conserved binary string is outputted, then one can be certain that an error occurred during computation and the result of the VQE can be disregarded.

2. Measurement

By decomposing the Hubbard Hamiltonian given in Eq. (4) into Pauli-strings, we end up with the following:

$$\begin{aligned}
H = & - \sum_{i,r,s} t_r (\sigma_{i+sL}^+ \sigma_{i+r+sL}^- + \sigma_{i+sL}^- \sigma_{i+r+sL}^+) \prod_{j=i+1+sL}^{i+r-1+sL} \sigma_j^z \\
& + \frac{1}{4} \sum_{i,r,s,s'} V_r \sigma_{i+sL}^z \sigma_{i+r+s'L}^z + \frac{U}{4} \sum_{i,s} \sigma_{i+sL}^z \sigma_{i+s'L}^z \\
& - \frac{1}{2} \left(N\lambda(\vec{V}) + \frac{N-1}{2}U \right) \sum_{i,s} \sigma_{i+sL}^z \\
& + \frac{NL}{2} \left(\frac{N}{2}\lambda(\vec{V}) + \frac{N-1}{4}U \right), \tag{8}
\end{aligned}$$

where

$$\lambda(\vec{V}) = \sum_{r=1}^{\lfloor \frac{L}{2} \rfloor} g_L(r) V_r, \quad (9)$$

with $\vec{V} = \{V_1, V_2, \dots, V_{\lfloor \frac{L}{2} \rfloor}\}$ and $g_L(r) = 1$ if $r < \frac{L}{2}$, or $1/2$ if $r = \frac{L}{2}$. Note that $\lambda(1) = \sum_{r=1}^{\lfloor \frac{L}{2} \rfloor} g_L(r)$ is the number of edges in a circulant graph [63] having edges of up to distance $\frac{L}{2}$ representative of the layout of a 1D ring lattice.

The Hubbard Hamiltonian thus consists of NL XX , YY , XY and YX terms, $NL(3N-1)/2$ ZZ terms, NL Z terms, and one constant term (which can be excluded from measurements), adding to a total of $3NL(N+3)/2$ measurement terms, meaning that naively taking separate energy measurements for each term in the Hamiltonian would prove to be severely error-prone. One solution to this problem is incorporating commuting sets of observables and measuring them in parallel [64, 65]. Immediately, it can be observed that the ZZ and Z terms can be measured in parallel, since they are already diagonal operators (and thus commuting) in the computational basis. The simplest way is to take the original form of $(I - Z_i)(I - Z_j)/4 = |11\rangle\langle 11|_{ij}$ for the ZZ terms and $(I - Z_i)/2 = |1\rangle\langle 1|_i$ for the Z terms, as given directly in Eq. (4). Hopping terms can be divided into three sets: **a**) the even-odd hopping terms, i.e. the terms in Eq. (7) acting on qubits 0-1, 2-3, 4-5, ..., **b**) the odd-even hopping terms, i.e. qubits 1-2, 3-4, 5-6, ..., and lastly **c**) the closed hopping term acting on qubits 0-($L-1$), along with the Z terms in between. To measure the hopping terms given in Eq. (7), a unitary operator that diagonalizes pairs of qubits in the hopping basis is given by

$$U_L(\phi) = \begin{pmatrix} 1 & 0 & 0 & 0 \\ 0 & \frac{1}{\sqrt{2}} & \frac{e^{i\frac{2\pi\phi}{L}}}{\sqrt{2}} & 0 \\ 0 & \frac{e^{i\frac{2\pi\phi}{L}}}{\sqrt{2}} & -\frac{e^{i\frac{4\pi\phi}{L}}}{\sqrt{2}} & 0 \\ 0 & 0 & 0 & 1 \end{pmatrix}. \quad (10)$$

This unitary operator is responsible for transforming the hopping terms in Eq. (7) to the diagonal basis $|01\rangle\langle 01| - |10\rangle\langle 10|$. It is significant to note that applying

sets of this transformation before measuring effectively increases the circuit depth by a further three CNOT gates [61].

This implies that only four sets of measurements are needed to calculate the expectation value of the Hamiltonian containing only nearest-neighbor hopping. It is also significant to note that if the number of spins for each color is odd, and the number of sites is even, then one can ignore the σ_z terms in between the closed hopping term, such as for example $(\sigma_L^+ \sigma_1^- + h.c.) \prod_{j=2}^{L-1} \sigma_j^z \rightarrow (\sigma_L^+ \sigma_1^- + h.c.)$, due to parity symmetry. This will enable the closed hopping term to fit in with the set of even-odd hopping terms, further reducing the total sets of measurements to three.

C. Results for $SU(4)$

Here we showcase results with matching parameters as in Fig. 2, but for the case of a commensurate $SU(4)$ Hubbard model. In Fig. 8, for small values of U and V (left panels), five layers are enough to capture the ground-state energy, yet for higher interaction terms (right panels) the VQE does not build up enough correlations in order to approximate the ground-state energy (see Fig. 4).

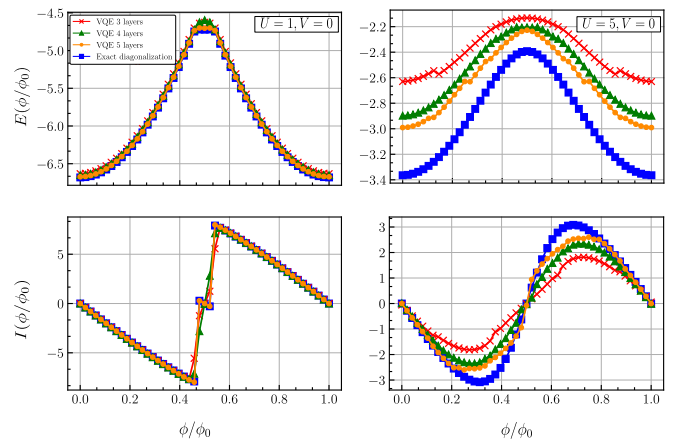


FIG. 8. The ground-state energy $E_0(\phi)$ (top panel) and the corresponding persistent current $I(\phi)$ (bottom panel) for $SU(4)$ fermions with different local U and nearest-neighbor V interactions, in the dilute filling regime of the Hubbard model. Exact diagonalization for $L = N_p = 4$ is used to monitor the results obtained by VQE.

[1] J. Preskill, Quantum computing in the nisq era and beyond, *Quantum* **2**, 79 (2018).
[2] K. Bharti, A. Cervera-Lierta, T. H. Kyaw, T. Haug, S. Alperin-Lea, A. Anand, M. Degroote, H. Heimonen, J. S. Kottmann, T. Menke, *et al.*, Noisy intermediate-scale quantum (NISQ) algorithms, arXiv:2101.08448 (2021).
[3] M. Cerezo, A. Arrasmith, R. Babbush, S. C. Benjamin, S. Endo, K. Fujii, J. R. McClean, K. Mitarai, X. Yuan, L. Cincio, *et al.*, Variational quantum algorithms, arXiv:2012.09265 (2020).

[4] J. Hubbard, Electron correlations in narrow energy bands, *Proceedings of the Royal Society of London. Series A. Mathematical and Physical Sciences* **276**, 238 (1963).

[5] F. H. L. Essler, H. Frahm, F. Göhmann, A. Klümper, and V. E. Korepin, *The One-Dimensional Hubbard Model* (Cambridge University Press, 2005).

[6] M. Lewenstein, A. Sanpera, V. Ahufinger, B. Damski, A. Sen, and U. Sen, Ultracold atomic gases in optical lattices: Mimicking condensed matter physics and beyond, *Advances in Physics* **56**, 243 (2007).

[7] A. Mazurenko, C. S. Chiu, G. Ji, M. F. Parsons, M. Kanász-Nagy, R. Schmidt, F. Grusdt, E. Demler, D. Greif, and M. Greiner, A cold-atom fermi-hubbard antiferromagnet, *Nature* **545**, 462 (2017).

[8] L. Tarruell and L. Sanchez-Palencia, Quantum simulation of the hubbard model with ultracold fermions in optical lattices, *Comptes Rendus Physique* **19**, 365 (2018).

[9] T. Esslinger, Fermi-hubbard physics with atoms in an optical lattice, *Annual Review of Condensed Matter Physics* **1**, 129 (2010).

[10] J. P. LeBlanc, A. E. Antipov, F. Becca, I. W. Bulik, G. K.-L. Chan, C.-M. Chung, Y. Deng, M. Ferrero, T. M. Henderson, C. A. Jiménez-Hoyos, *et al.*, Solutions of the two-dimensional hubbard model: Benchmarks and results from a wide range of numerical algorithms, *Physical Review X* **5**, 041041 (2015).

[11] T. Hensgens, T. Fujita, L. Janssen, X. Li, C. Van Diepen, C. Reichl, W. Wegscheider, S. D. Sarma, and L. M. Vandersypen, Quantum simulation of a fermi-hubbard model using a semiconductor quantum dot array, *Nature* **548**, 70 (2017).

[12] C. Cade, L. Mineh, A. Montanaro, and S. Stanisic, Strategies for solving the fermi-hubbard model on near-term quantum computers, *Physical Review B* **102**, 1 (2020).

[13] Z. Cai, Resource estimation for quantum variational simulations of the hubbard model, *Physical Review Applied* **14**, 1 (2020).

[14] D. S. Abrams and S. Lloyd, Simulation of many-body fermi systems on a universal quantum computer, *Physical Review Letters* **79**, 2586 (1997).

[15] P. L. Dallaire-Demers and F. K. Wilhelm, Method to efficiently simulate the thermodynamic properties of the fermi-hubbard model on a quantum computer, *Physical Review A* **93**, 1 (2016).

[16] B. Bauer, D. Wecker, A. J. Millis, M. B. Hastings, and M. Troyer, Hybrid quantum-classical approach to correlated materials, *Physical Review X* **6**, 1 (2016).

[17] J.-M. Reiner, F. Wilhelm-Mauch, G. Schön, and M. Marthaler, Finding the ground state of the hubbard model by variational methods on a quantum computer with gate errors, *Quantum Science and Technology* **4**, 035005 (2019).

[18] A. Uvarov, J. D. Biamonte, and D. Yudin, Variational quantum eigensolver for frustrated quantum systems, *Physical Review B* **102**, 075104 (2020).

[19] A. Peruzzo, J. McClean, P. Shadbolt, M.-H. Yung, X.-Q. Zhou, P. J. Love, A. Aspuru-Guzik, and J. L. O'brien, A variational eigenvalue solver on a photonic quantum processor, *Nature communications* **5**, 1 (2014).

[20] R. W. Cherng, G. Refael, and E. Demler, Superfluidity and magnetism in multicomponent ultracold fermions, *Physical Review Letters* **99**, 130406 (2007).

[21] A. Rapp, G. Zaránd, C. Honerkamp, and W. Hofstetter, Color superfluidity and “baryon” formation in ultracold fermions, *Physical Review Letters* **98**, 160405 (2007).

[22] A. Keller, S. Amasha, I. Weymann, C. Moca, I. Rau, J. Katine, H. Shtrikman, G. Zaránd, and D. Goldhaber-Gordon, Emergent $su(4)$ kondo physics in a spin-charge-entangled double quantum dot, *Nature Physics* **10**, 145 (2014).

[23] K. Kugel, D. Khomskii, A. Sboychakov, and S. Streltsov, Spin-orbital interaction for face-sharing octahedra: Realization of a highly symmetric $su(4)$ model, *Physical Review B* **91**, 155125 (2015).

[24] K. Nomura and A. H. MacDonald, Quantum hall ferromagnetism in graphene, *Physical Review Letters* **96**, 256602 (2006).

[25] D. Arovas, A. Karlhede, and D. Lilliehöök, $Su(n)$ quantum hall skyrmions, *Physical Review B* **59**, 13147 (1999).

[26] S. Capponi, P. Lecheminant, and K. Totsuka, Phases of one-dimensional $su(n)$ cold atomic fermi gases –from molecular luttinger liquids to topological phases, *Annals of Physics* **367**, 50 (2016).

[27] M. A. Cazalilla and A. M. Rey, Ultracold fermi gases with emergent $su(n)$ symmetry, *Reports on Progress in Physics* **77**, 124401 (2014).

[28] T. Sowiński and M. Á. García-March, One-dimensional mixtures of several ultracold atoms: a review, *Reports on Progress in Physics* **82**, 104401 (2019).

[29] G. Pagano, M. Mancini, G. Cappellini, P. Lombardi, F. Schäfer, H. Hu, X. J. Liu, J. Catani, C. Sias, M. Inguscio, *et al.*, A one-dimensional liquid of fermions with tunable spin, *Nature Physics* **10**, 198 (2014).

[30] G. Cappellini, M. Mancini, G. Pagano, P. Lombardi, L. Livi, M. Siciliani de Cumis, P. Cancio, M. Pizzocaro, D. Calonico, F. Levi, *et al.*, Direct observation of coherent interorbital spin-exchange dynamics, *Physical Review Letters* **113**, 120402 (2014).

[31] F. Scazza, C. Hofrichter, M. Höfer, P. De Groot, I. Bloch, and S. Fölling, Observation of two-orbital spin-exchange interactions with ultracold $su(n)$ -symmetric fermions, *Nature Physics* **10**, 779 (2014).

[32] L. Amico, M. Boshier, G. Birk, A. Minguzzi, C. Miniatura, L. C. Kwek, D. Aghamalyan, V. Ahufinger, D. Anderson, N. Andrei, *et al.*, State of the art and perspective on atomtronics, *arXiv:2008.04439* (2021).

[33] W. J. Chetcuti, T. Haug, L.-C. Kwek, and L. Amico, Persistent current of $su(n)$ fermions, *arXiv:2011.00916* (2020).

[34] B. S. Shastry, Infinite conservation laws in the one-dimensional hubbard model, *Physical Review Letters* **56**, 1529 (1986).

[35] J.-M. Reiner, M. Marthaler, J. Braumüller, M. Weides, and G. Schön, Emulating the one-dimensional fermi-hubbard model by a double chain of qubits, *Physical Review A* **94** (2016).

[36] S. Xu, J. T. Barreiro, Y. Wang, and C. Wu, Interaction effects with varying n in $su(n)$ symmetric fermion lattice systems, *Physical Review Letters* **121**, 167205 (2018).

[37] A. P. R. Alcázar, R. Franco, and J. Silva-Valencia, Phase diagram of the $su(3)$ fermi-hubbard model with next-neighbor interactions, *arXiv:2004.11249* (2020).

[38] S. McArdle, S. Endo, A. Aspuru-Guzik, S. C. Benjamin, and X. Yuan, Quantum computational chemistry, *Reviews of Modern Physics* **92**, 15003 (2020).

[39] P. L. Dallaire-Demers and F. K. Wilhelm, Quantum gates and architecture for the quantum simulation of the fermi-hubbard model, *Physical Review A* **94**, 1 (2016).

[40] P. Jordan and E. Wigner, Über das Paulische Äquivalenzverbot, *Zeitschrift fur Physik* **47**, 631 (1928).

[41] A. Garcia-Saez and J. Latorre, Addressing hard classical problems with adiabatically assisted variational quantum eigensolvers, *arXiv:1806.02287* (2018).

[42] S. Efthymiou, S. Ramos-Calderer, C. Bravo-Prieto, A. Pérez-Salinas, D. García-Martín, A. Garcia-Saez, J. I. Latorre, and S. Carrazza, Qibo: a framework for quantum simulation with hardware acceleration, *arXiv:2009.01845* (2020).

[43] S. Efthymiou, S. Ramos-Calderer, C. Bravo-Prieto, A. Pérez-Salinas, D. García-Martín, A. Garcia-Saez, J. I. Latorre, and S. Carrazza, Quantum-tii/qibo: Qibo (2020).

[44] J. Nocedal and S. Wright, *Numerical optimization* (Springer Science & Business Media, 2006).

[45] P. Weinberg and M. Bukov, Quspin: a python package for dynamics and exact diagonalisation of quantum many body systems part i: spin chains, *SciPost Physics* **2**, 003 (2017).

[46] P. Weinberg and M. Bukov, Quspin: a python package for dynamics and exact diagonalisation of quantum many body systems. part ii: bosons, fermions and higher spins, *SciPost Physics* **7**, 020 (2019).

[47] C. Bravo-Prieto, J. Lumbrales-Zarapico, L. Tagliacozzo, and J. I. Latorre, Scaling of variational quantum circuit depth for condensed matter systems, *Quantum* **4**, 272 (2020).

[48] S. B. Bravyi and A. Y. Kitaev, Fermionic quantum computation, *Annals of Physics* **298**, 210 (2002).

[49] R. C. Ball, Fermions without fermion fields, *Physical Review Letters* **95**, 1 (2005).

[50] F. Verstraete and J. I. Cirac, Mapping local hamiltonians of fermions to local hamiltonians of spins, *Journal of Statistical Mechanics: Theory and Experiment* **2005**, P09012-p09012 (2005).

[51] M. Sun and M. R. Geller, Efficient characterization of correlated spam errors, *arXiv:1810.10523* (2020).

[52] Contextual optimization, https://cqcl.github.io/pytket/build/html/manual/manual_compiler.html#contextual-optimisations (2021).

[53] J. Decamp, P. Armagnat, B. Fang, M. Albert, A. Minguetti, and P. Vignolo, Exact density profiles and symmetry classification for strongly interacting multi-component fermi gases in tight waveguides, *New Journal of Physics* **18**, 055011 (2016).

[54] P. Nataf and F. Mila, Exact diagonalization of heisenberg $SU(n)$ chains in the fully symmetric and antisymmetric representations, *Phys. Rev. B* **93**, 155134 (2016).

[55] J. J. Wallman and J. Emerson, Noise tailoring for scalable quantum computation via randomized compiling, *Physical Review A* **94** (2016).

[56] G. White, C. Hill, and L. Hollenberg, Performance optimization for drift-robust fidelity improvement of two-qubit gates, *Physical Review Applied* **15** (2021).

[57] R. Orús, Tensor networks for complex quantum systems, *Nature Reviews Physics* **1**, 538 (2019).

[58] B. Bruognolo, J.-W. Li, J. von Delft, and A. Weichselbaum, A beginner's guide to non-abelian ipeps for correlated fermions, *SciPost Physics Lecture Notes* **25**, 25 (2021).

[59] S. Ramos-Calderer, C. Bravo-Prieto, M. Consiglio, and W. J. Chetcuti, <https://github.com/qiboteam/vqe-sun> (2021).

[60] D. Willsch, M. Nocon, F. Jin, H. De Raedt, and K. Michielsen, Gate-error analysis in simulations of quantum computers with transmon qubits, *Physical Review A* **96** (2017).

[61] F. Vatan and C. Williams, Optimal quantum circuits for general two-qubit gates, *Physical Review A* **69** (2004).

[62] M. Möttönen and J. J. Vartiainen, Decompositions of general quantum gates, *Trends in Quantum Computing Research* (2006).

[63] E. W. Weisstein, Circulant graph, <https://mathworld.wolfram.com/CirculantGraph.html> (2021).

[64] A. Jena, S. Genin, and M. Mosca, Pauli partitioning with respect to gate sets, *arXiv:1907.07859* (2019).

[65] A. Zhao, A. Tranter, W. M. Kirby, S. F. Ung, A. Miyake, and P. J. Love, Measurement reduction in variational quantum algorithms, *Physical Review A* **101**, 1 (2020).